Supplementary Information

$CoFe_2O_4$-ZnS nanocomposite: a magnetically recyclable photocatalyst

Kula Kamal Senapati, Chandan Borgohain, and Prodeep Phukan
Department of Chemistry, Gauhati University, Guwahati, 781014, Assam, India.
E-mail: pphukan@yahoo.com

Synthesis of ZnS nanoparticles.

Prior to coating of ZnS NPs to $CoFe_2O_4$ surface, ZnS NPs were synthesized by slightly modified method reported by N. Saravanan et al.[1] A solution of 0.1 M zinc chloride, 0.1 M sulphur powder, 5 M NaOH in 100 mL deionised distilled water was ultrasonicated for 2 h at 80 ^oC under argon atmosphere. The product was then separated by centrifugation at 14000 rpm, washed several times with distilled deionized water and finally dried under vacuum.

Synthesis of $CoFe_2O_4$ -ZnS nanocomposite.

The synthesis of $CoFe_2O_4$ MNPs were carried out following the reported method.[2]

The optimal concentration of Co^{2+}, Fe^{3+} and a mixed surfactant (total concentration of oleic acid/dodecylamine, designated as [OA + DA] was $[Co^{2+}]$ = 0.2 M, $[Fe^{3+}]$ = 0.4 M, and [OA + DA] = 4 M. In a typical procedure, absolute ethanol (20 mL) was mixed with 1:1 adduct of oleic acid and dodecylamine under magnetic stirring for 15 min to form homogeneous **solution I**.

In the next step, a solution of $CoCl_2.6H_2O$ (1g, 4.2 mmol) in distilled water (50 mL) was mixed with a solution of $FeCl_3$ (1.5 g, 9.3 mmol) in distilled water (50 mL) in a two-neck 200 mL flat bottom flask and kept under ultrasonication for 30 min in argon atmosphere. Then this mixture was added drop wise to **solution I** under magnetic stirring. The whole mixture was kept in an ultrasonic bath and an aqueous KOH solution (3 M, 25 mL) was added drop-wise under argon atmosphere with continuous ultrasonic irradiation (frequency 40 KHz and power of 40 KW). The temperature of the sonicator bath was raised up to 60 ^oC and the mixture was further sonicated for 1 h till the formation of black particles was observed. Thereafter, the reaction mixture was allowed to cool to room temperature and the product was collected by centrifugation (20000 rpm) at ambient temperature. The separated oleic acid-dodecylamine coated $CoFe_2O_4$ nanoparticles were washed several times with distilled water and finally with ethanol to get rid of excess surfactants as confirmed by EDX analysis. Then a specific amount of ZnS NPs dispersed in de-ionized water was added to the dispersion of oleic acid-dodecyl amine coated $CoFe_2O_4$ NPs in de-ionized water under vigorous sonication for 1 h. The precipitates were further washed with ethanol (4 times) so as to remove excess ZnS particles in the final product. Finally, the precipitate was dried at 400 °C under nitrogen purging for 6 h to obtain the $CoFe_2O_4$-ZnS core-

shell structure. The dried $CoFe_2O_4$-ZnS NCs were kept under vacuum till further use. The as synthesized nanocomposites could be easily redispersed in aqueous medium.

Preparation of TiO_2 Nanoparticles

The TiO_2 NPs having both the anatase and rutile phase were prepared by the reported method of H. Yang et al.[3]

The starting materials were AR-grade $Ti(OBu_4)$ and anhydrous alcohol. 10 mL of $Ti(OBu_4)$ was dissolved in 10 mL anhydrous alcohol, and ultrasonicated to produce a dispersed mixture. 5 mL of water was slowly added into the mixture, which was stirred for 2 h at room temperature. The pH value of the solution was maintained to be 3.0. The solution was aged for 24 h at ambient temperature, followed by filtering, washing for several times with deionized water and anhydrous alcohol, drying at 100 ^oC for 12 h to form a precursor. Subsequent calcination of the precursor at 650 ^oC for 2 h in air resulted in the formation of TiO_2 NPs.

Characterization of nanoparticles

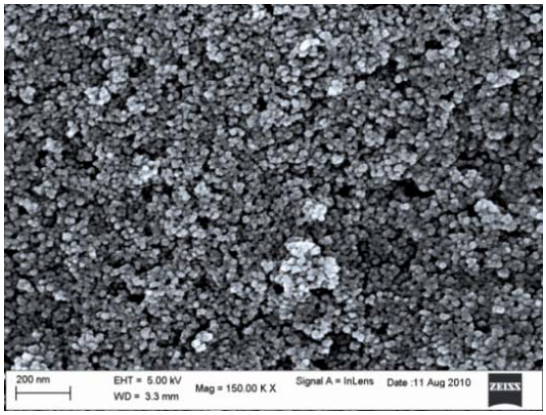

Figure S1. FESEM morphology of $CoFe_2O_4$-ZnS NCs at magnification of 150 KX.

The bright field TEM image (**Figure S2 a-b**) clearly shows the $CoFe_2O_4$ MNPs decorated with a outer layer of very small particles, attributed to ZnS. Thus the nanocomposites has a discrete core-shell structure with the surface of $CoFe_2O_4$ crystals becomes coated with an uniform thin layer of ZnS nanoparticles. The average size of the nanocomposites from the TEM analysis was found to be 30±5 nm.

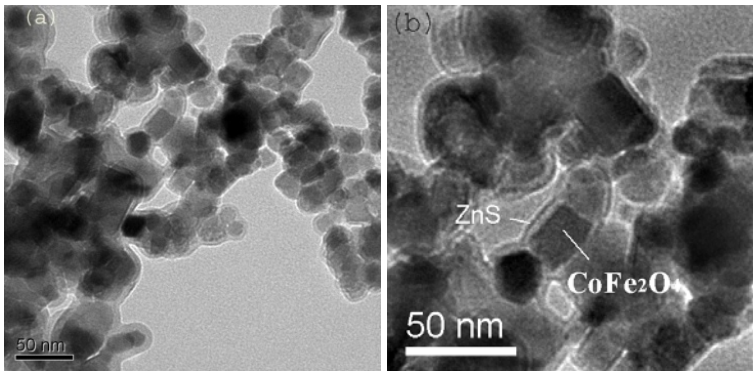

Figure S2. Morphology of $CoFe_2O_4$-ZnS NCs (a) TEM and (b) IFFT of TEM.

The SAED pattern in **Figure S3a** showed the diffractions from the lattice planes of $CoFe_2O_4$ and ZnS. The spots labeled as 1, 2, and 4 are the respective (111), (220) and (311) planes of spinel $CoFe_2O_4$ MNPs and 3 and 5 are the respective (111) and (311) planes of cubic ZnS NPs.

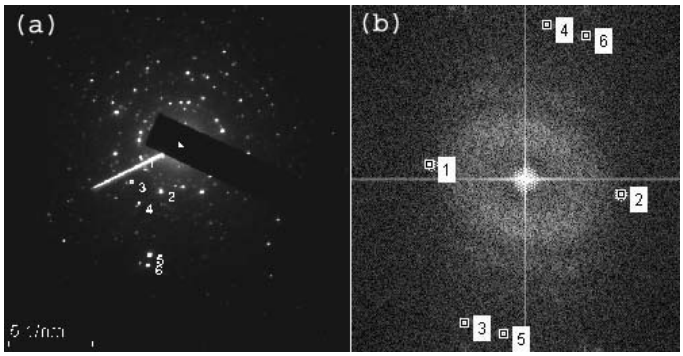

Figure S3. (a) SAED pattern and (b) FFT of the SAED pattern

The lattice image of the nanocomposite (**Figure S4a-b**) marked with the lattice plane (111) of spinel $CoFe_2O_4$ and (220) of cubic ZnS NPs revealed the highly crystalline nature of the nanocomposites. The high resolution TEM (HRTEM) image allowed us, by means of Gatan Digital Micrograph^{TM} software, to obtain the fast Fourier transform (FFT) from which lattice spacings of 4.59 A° and 2.7 A° were obtained (experimental error, <5%) for the $CoFe_2O_4$ and ZnS nanoparticles respectively. These lattice spacings of the nanocomposites were taken at the interface of the core and shell materials of the nanocomposites as depicted in **Figure S4b**.

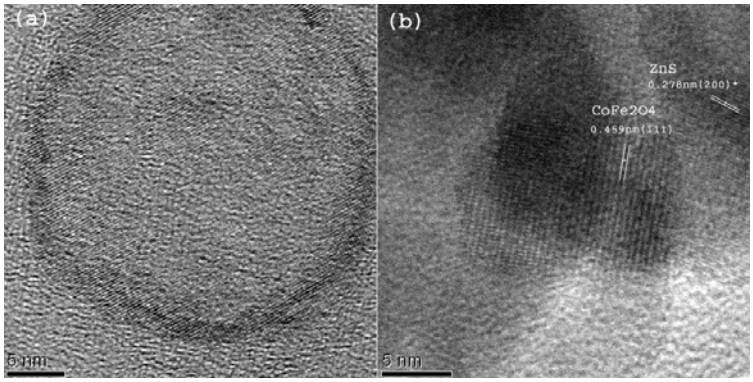

Figure S4. HRTEM image of $CoFe_2O_4$-ZnS core shell NCs showing (a) Core-shell structure and (b) Lattice image marked with lattice planes.

The lattice planes in the HRTEM image (**Figure S5a**) was further separated and replotted in **Figure S5(c-d)** by using IFFT (**Figure S5b**) and masking techniques using the Gatan Digital Micrograph™ Software. The separated lattice planes were clearly visualized and labeled as (111) and (200) planes of the respective core and shell materials at the interface of the nanocomposites.

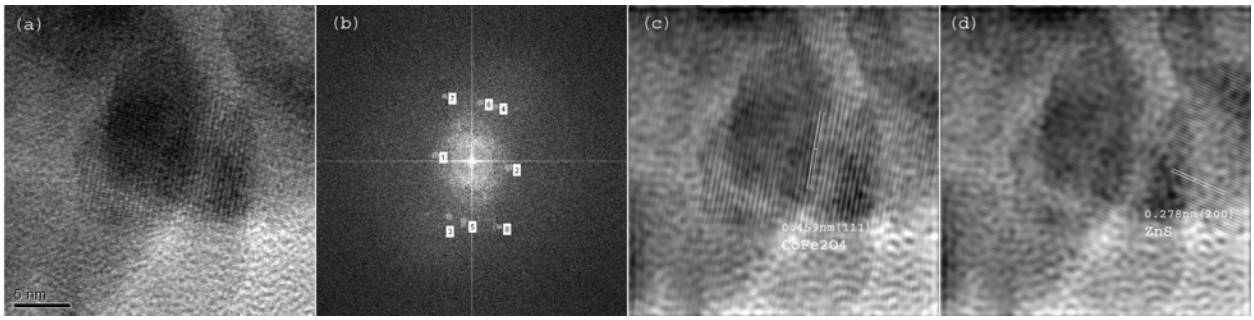

Figure S5. Lattice planes of $CoFe_2O_4$-ZnS NCs (a) Core-shell interface, (b) IFFT of HRTEM, (c) (111) plane of $CoFe_2O_4$ and (d) (200) plane of ZnS.

Band-gap Energy

The band-gap energy of the as-synthesized nanocomposite was evaluated from the UV-vis measurement. The UV-vis spectrum of colloidal solution of the $CoFe_2O_4$-ZnS shows absorption bands at around 280 nm. The band-gap energy, Eg corresponding to the absorption band was determined from the absorbance spectra, where a steep increase in the absorption was observed due to the band-band transition using the relation.

$$(\alpha h\nu)^n = B(E-Eg)$$

Where B is a constant related to the effective masses of charge carriers associated with valance and conduction bans, Eg the band-gap energy, E= $h\nu$ the photon energy, and n=1/2 or 2, depending on whether the transition is indirect or direct, respectively. The intersection of the slope of $(\alpha h\nu)^2$ vs $h\nu$ curve on the x-axis gives band-gap energy of the sample. The Tauc plot for

the $CoFe_2O_4$-ZnS nanocomposite is depicted in the inset of Figure 3 and the band-gap energy was found to be 3.2 eV.

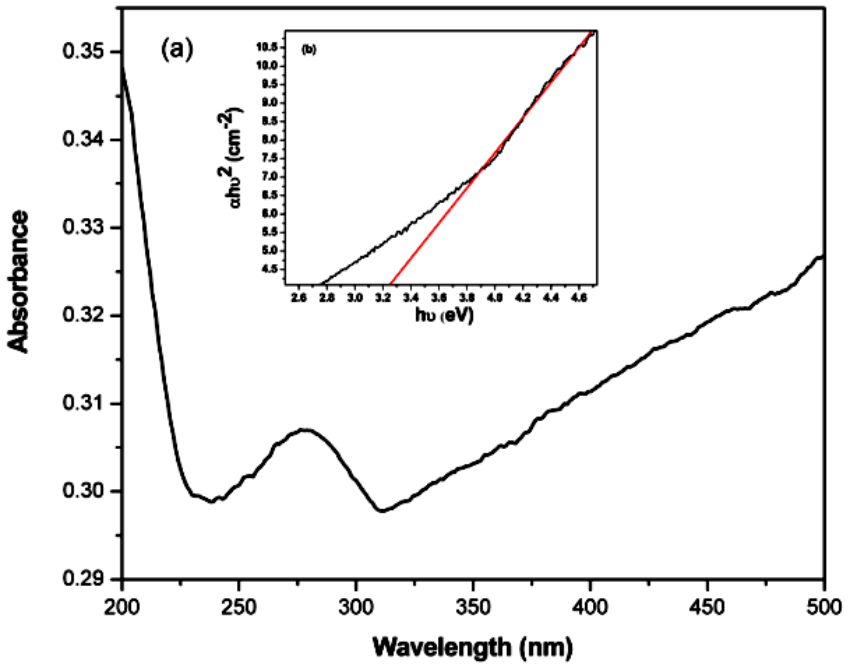

Figure S6. UV-Vis absorbance spectra of $CoFe_2O_4$ ZnS NCs and inset figure is the Tauc plot i.e the plot of $(\alpha h\upsilon)^2$ vs. Photon energy ($h\upsilon$).

Characterization of TiO_2 nanoparticles

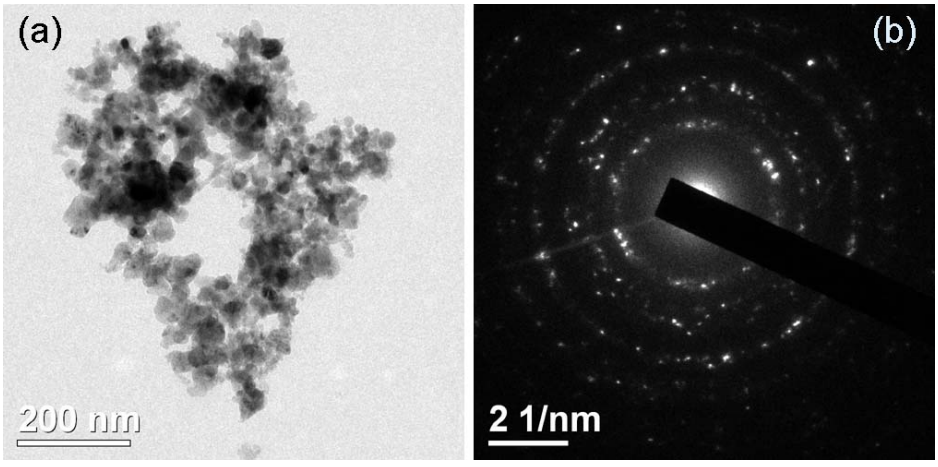

Figure S7. (a) TEM image and (b) SAED pattern of TiO_2 NPs

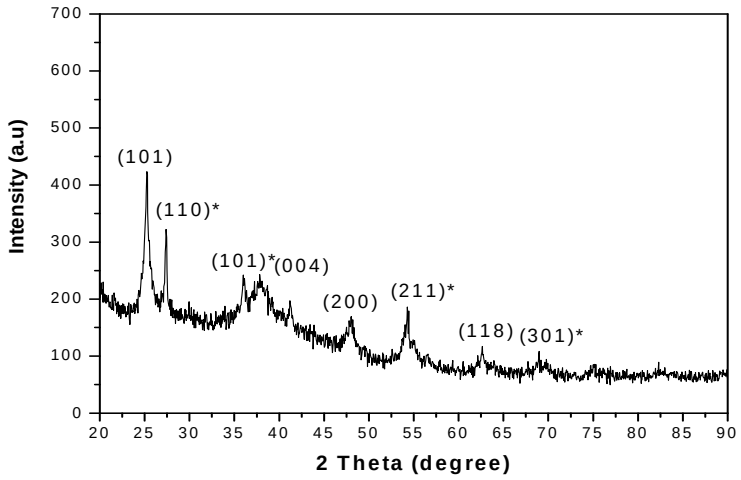

Figure S8. XRD pattern of as prepared TiO_2 NPs

In Figure S8, XRD pattern shows strong diffraction peaks (marked by *) at 27°, 36° and 55° indicating TiO_2 in the rutile phase. The XRD pattern also exhibits strong diffraction peaks at 25° and 48° indicating TiO_2 in the anatase phase. All peaks are in good agreement with the standard spectrum (JCPDS no.: 88-1175 and 84-1286). Thus the crystalline phase of the as prepared sample shows peaks characteristic of both the anatase and rutile phase.

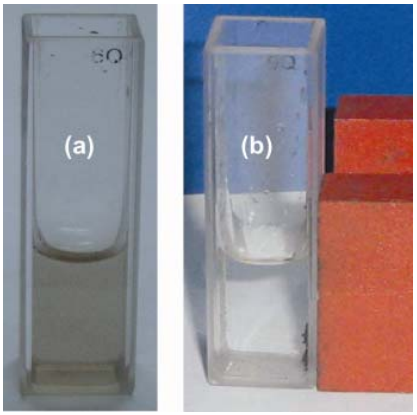

Figure S9. $CoFe_2O_4$-ZnS NCs in its (a) aqueous dispersion and (b) magnetic separation

Liquid Chromatography Mass Spectrometry

Experimental

The LCMS analysis (Waters Q-Tof Premier LC MS/MS system) was performed with a binary pump, T-UV-Vis diode array detector, an autosampler, and a column thermostat. The LCMS system was equipped with a C18 column (Acquity UPLC^{TM} BEH C18 1.7 um, 2.1x50mm Column). The solvent used as mobile phase was acetonitrile: water (1:1). The flow rate was 0.3 mL min^{-1} and 30 uL of standard or sample solution was injected through the column. High purity nitrogen (99.99%) and argon (99.999%) was used as nebulizer (API gas) and collision cell gas respectively. The gradient HPLC separation was coupled with LC/Mass. The mass spectrometer source was electrospray ionization (ESI) and operated at negative polarity. The ESI conditions were as follows: capillary voltage: 2.5 kV, source temperature: 100 ^{o}C. cone voltage: 20V collision energy 5-30 eV. The mass range scan was from 100 to 500 m/z. The Tandem Mass analysis was done using argon as collision gas selecting 304 as precursor mass.

Mass analysis

The liquid chromatography coupled with mass spectrometry was used for the degradation experiment. The fragmentation of methyl orange (MO) was studied by tandem mass spectrometry (MS/MS) experiments, where the MO precursor ion is isolated first by the mass analyzer, then collision activation of the ion is performed yielding the fragment ions. The MS/MS of MO increases the specificity of detection because there is no uncertainty in the product ion spectrum.

The parent molecule of MO gave a signal corresponding to a negative ion at m/z 304 $[M-H]^-$ as shown in ESI-Mass spectrum (**Figure S10a**).[1] The MS/MS spectrum of this ion gave three significant fragment peaks at m/z values of 288, 240, and 156 (**Figure S10b**). The fragment ion at m/z 288 was derived from the cleavage of one methyl group. The fragment ion at m/z 240 was derived from the cleavage of a sulphonate group. The ion at m/z 156 was corresponded to $[M-H-N_2C_6H_4N(CH_3)_2]^-$. The sum of MS/MS product ions at m/z 288, 240, and 156 was for the determination of MO residues.

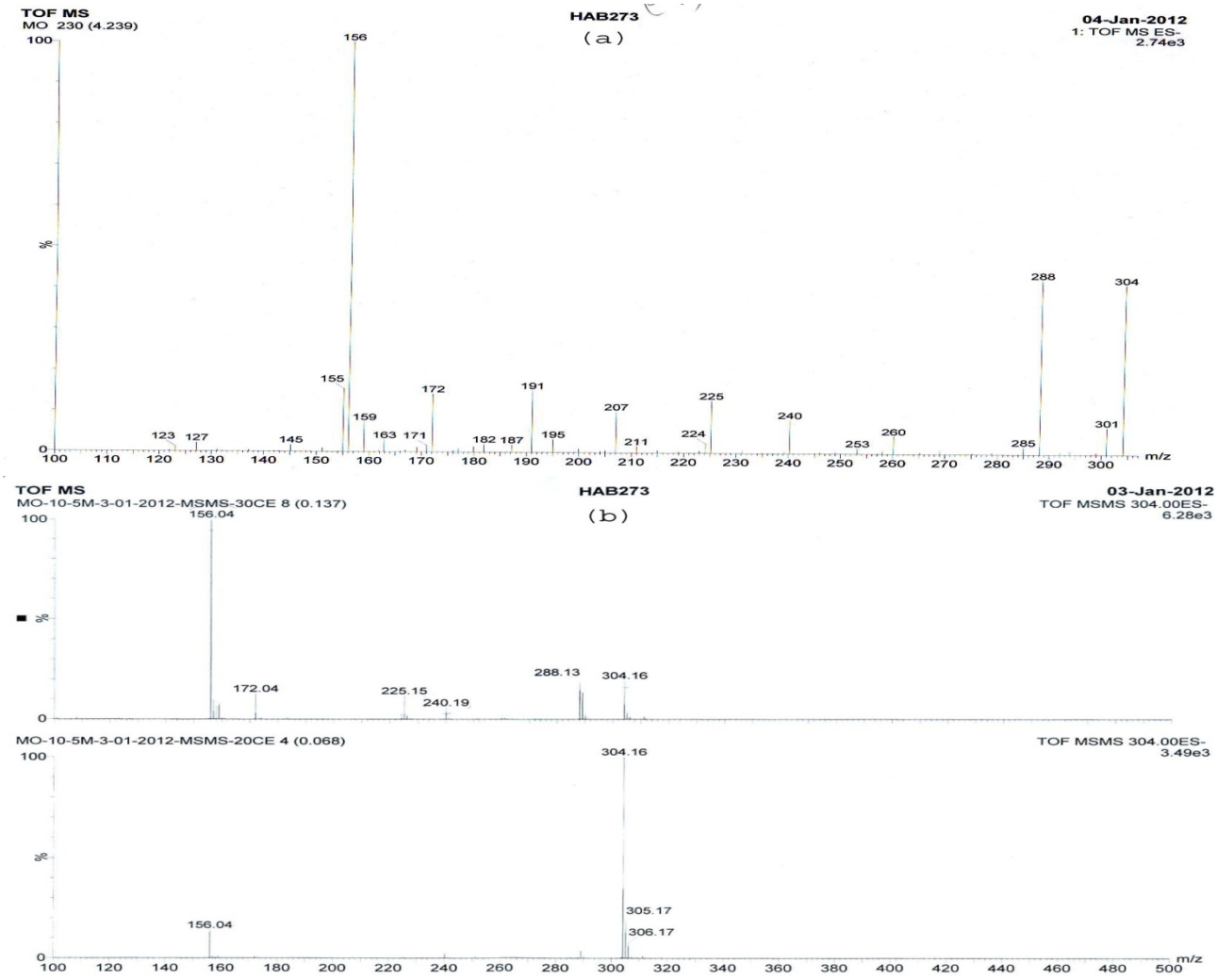

Figure S10. (-) ESI mass spectra of MO (a) First order and (b)Tandem mass spectra (MS/MS of m/z 304).

Figure S11 shows the ESI-Mass spectra of MO solution after degradation of 20 min under UV irradiation in presence of the catalyst. No peaks were detected for the parent molecular ion (m/z 304) or its normal fragmentation products (m/z 288, 240) which revealed that the destruction of MO molecule occurred under the reaction conditions applied. Very low intensity peaks at m/z 155 and 169 were detected due to the fragmented ions of small molecules. The peak at m/z 113 existed in the course of LCMS operation; perhaps it was due to the impurity in the solvent used.

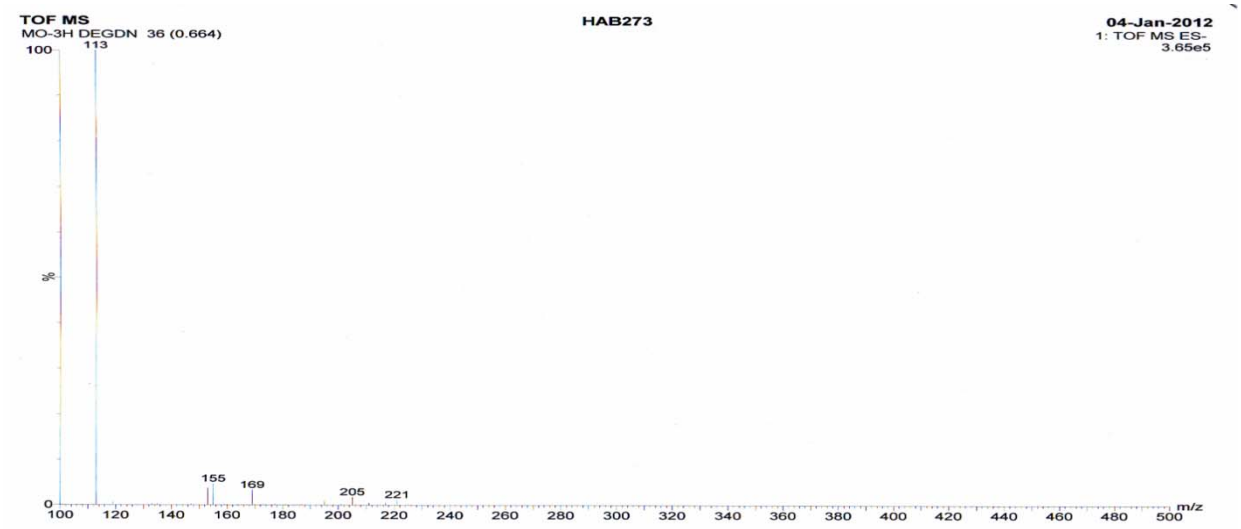

Figure S11. (-) ESI mass spectra of MO after degradation (20 min)

LC-UV-Vis measurement for product analysis

The chromatographic separation of the MO solution recorded initially and after 20 min of photocatalytic treatment was monitored at the dual wavelengths of 254 nm and 460 nm and is shown in **Figure S12** and **Figure S13** respectively. The MO solution gave two significant peaks at retention times (r.t) 0.63 min and 4.24 min corresponding to the solvent and MO molecules as shown in **Figure S12a** with their extracted mass in the inset. The **Figure S12b** showed the LC profile with UV chromatogram as detected by diode array detector (TUV detector) of the MO solution before degradation which gave absorption peak of the maximum intensity at r.t 0.42 min and wavelength length 460 nm. However, we didn't observe the peak of significant intensity for the MO solution after the degradation at r.t 4.2 min except the peak at r.t 0.68 min (**Figure S13a**) which was due to the solvent present in MO solution before and after the degradation. Moreover, the LC-UV chromatogram in **Figure S13b** shows no absorption peak of MO and only the maximum absorption was detected at the wavelength of 254 nm which was attributed from the solvent and its contamination. This experimental data implied that at the end of 20 min irradiation, the MO was significantly degraded. This is evident by the nonappearance of the MO peak of considerable intensity and the absence of new peaks at lower retention times corresponding to new photocatalytic products of the MO. Consequently, photocatalysis of MO solutions not only caused its decoloration, but also an appreciable degree of destruction in the molecule. Therefore, the liquid chromatography coupled with UV absorbance using diode array detector clearly showed that, the MO was appreciably degraded into small molecules such as CO_2, NH_4, SO_2 , N_2 etc. which could not be detected by LCMS analysis.

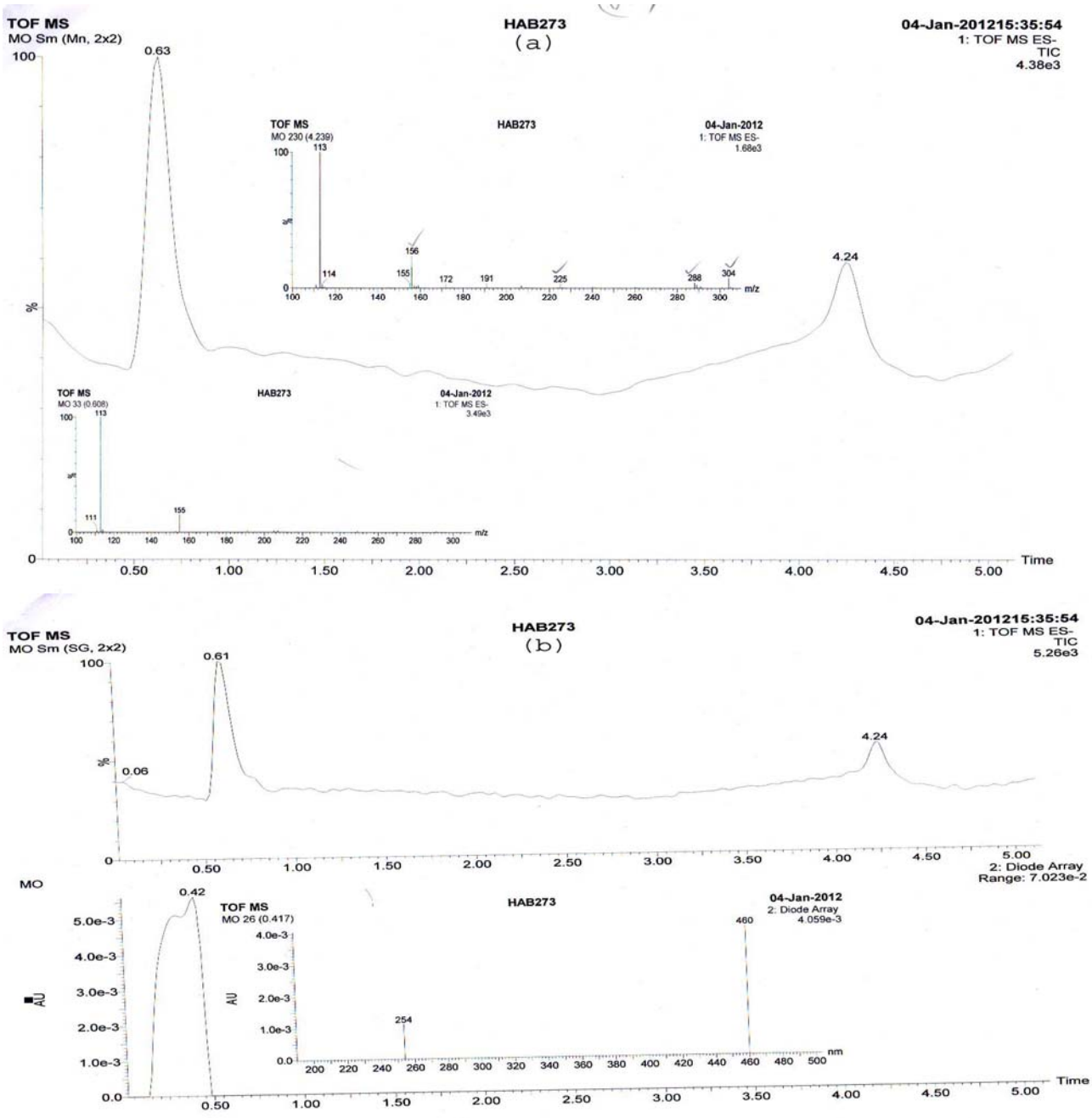

Figure S12. LC profile of MO with (a) extracted mass (MS) at different retention time and (b) UV chromatogram before degradation

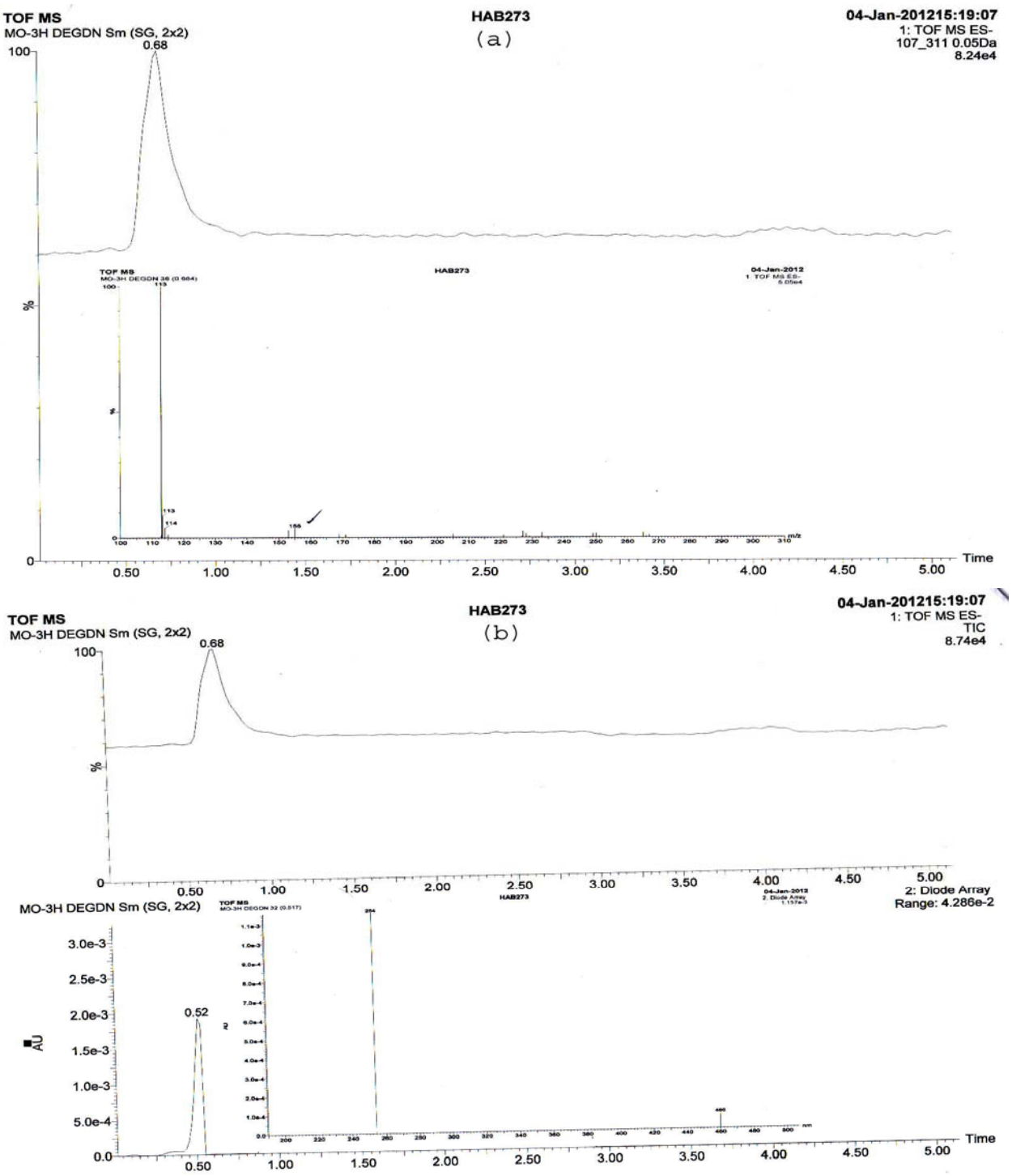

Figure S13. LC profile of MO with (a) extracted mass (MS) at different retention time and (b) UV chromatogram after degradation

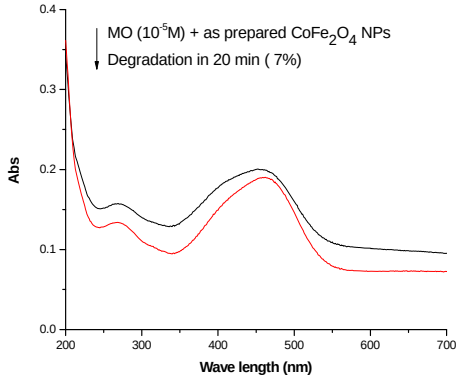

Figure S14. Degradation of methyl orange by as prepared $CoFe_2O_4$ MNPs

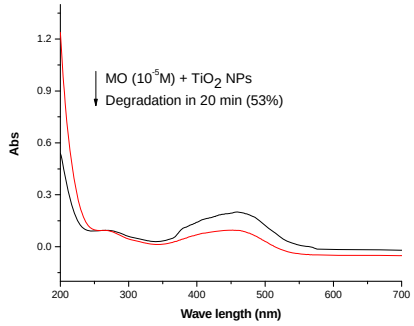

Figure S15. Degradation of methyl orange by as prepared TiO_2 NPs

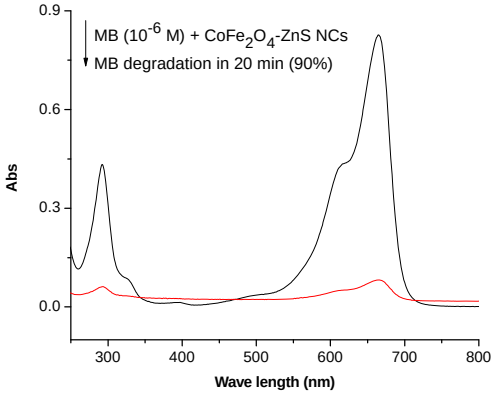

Figure S16. Degradation of methylene blue by as prepared $CoFe_2O_4$-ZnS NCs

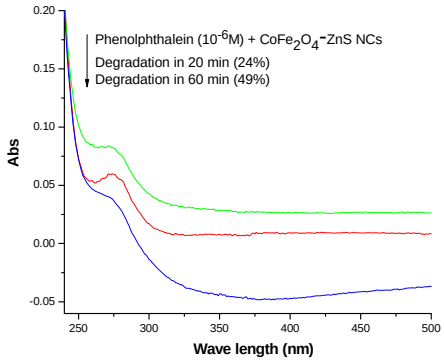

Figure S17. Degradation of phenolpthalein by as prepared $CoFe_2O_4$-ZnS NCs

The high dispersability and stability of the $CoFe_2O_4$–ZnS nanocomposite in aqueous medium was also inferred from the optical absorbance measurements taken at different time intervals as we reported in case of nanoparticles of $CoFe_2O_4$ and $CoFe_2O_4$–Cr_2O_3–SiO_2 NPs prepared under ultrasonic treatment.[2] It was observed that there were no considerable changes in absorbance spectra of the aqueous dispersion of $CoFe_2O_4$–ZnS up to 1 h under the same photocatalytic condition.

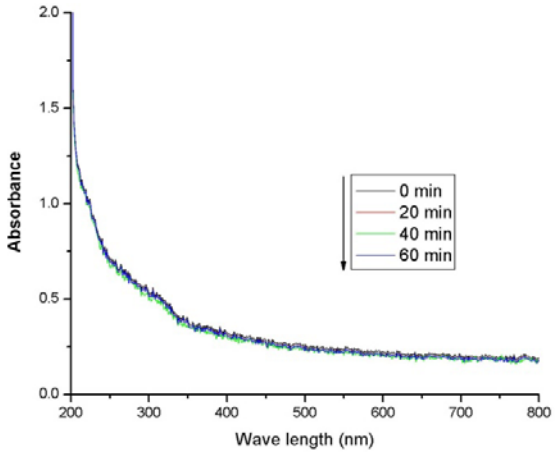

Figure S18. UV-Vis absorbance spectra of aqueous dispersion of $CoFe_2O_4$–ZnS NCs

References

1. N. Saravanan , G. B. Teh, S. Y. P. Yap , K. M. Cheong, *J Mater Sci: Mater Electron* 2008, **19**, 1206.
2. (a) K. K. Senapati, C. Borgohain, K. C. Sarma, P. Phukan, *J Mol Cat. A: Chemical* 2011, **339**, 24.; (b) C. Borgohain, K. K. Senapati, D. Mishra, K. C. Sarma, P. Phukan, *Nanoscale* 2011, **2**, 2250.
3. H. Yang, K. Zhang, R. Shi, X. Li, X. Dongb, Y. Yu, *J. Alloys Comp.* 2006, **413**, 302.